Spatiotemporal control of cardiac alternans

Blas Echebarria, and Alain Karma

Citation: Chaos **12**, 923 (2002); doi: 10.1063/1.1501544
View online: https://doi.org/10.1063/1.1501544
View Table of Contents: http://aip.scitation.org/toc/cha/12/3
Published by the American Institute of Physics

Spatiotemporal control of cardiac alternans

Blas Echebarria and Alain Karma
Department of Physics and Center for Interdisciplinary Research on Complex Systems, Northeastern University, Boston, Massachusetts 02115

(Received 10 June 2002; accepted 28 June 2002; published 23 August 2002)

Electrical alternans are believed to be linked to the onset of life-threatening ventricular arrhythmias and sudden cardiac death. Recent studies have shown that alternans can be suppressed temporally by dynamic feedback control of the pacing interval. Here we investigate theoretically whether control can suppress alternans both temporally and spatially in homogeneous tissue paced at a single site. We first carry out ionic model simulations in a one-dimensional cable geometry which show that control is only effective up to a maximum cable length that decreases sharply away from the alternans bifurcation point. We then explain this finding by a linear stability analysis of an amplitude equation that describes the spatiotemporal evolution of alternans. This analysis reveals that control failure above a critical cable length is caused by the formation of standing wave patterns of alternans that are eigenfunctions of a forced Helmholtz equation, and therefore remarkably analogous to sound harmonics in an open pipe. We discuss the implications of these results for using control to suppress alternans in the human ventricles as well as to probe fundamental aspects of alternans morphogenesis. © *2002 American Institute of Physics.* [DOI: 10.1063/1.1501544]

At sufficiently fast pacing rates, the duration of cardiac electrical excitation is often observed to oscillate from beat to beat. Several theoretical and experimental studies to date support the hypothesis that the resulting sequence of long-short-long-short action potential duration, termed alternans, is closely linked to the onset of the turbulent electrical activity known as ventricular fibrillation, which stops the heart from pumping and leads to sudden cardiac death. It is therefore practically relevant to determine if alternans can be controlled by some implantable pacing device that continuously monitors the electrical activity of the heart. Recent studies have demonstrated that alternating heart rhythms associated with a period doubling instability can be suppressed by comparing the electrical response of the tissue at subsequent beats and modifying accordingly the interval between stimuli. Here we investigate whether such a feedback scheme can control alternans both temporally and spatially in cardiac tissue paced from one site. We show that the largest tissue size that can be controlled is severely limited by the formation of standing waves of alternans that are analogous to sound wave harmonics.

I. INTRODUCTION

When heart cells are paced rapidly, they often exhibit a beat-to-beat oscillation of the duration of the action potential (electrical impulse) that signals their contraction; that is, an alternating sequence of long-short-long-short action potential duration (APD).[1] On the scale of the whole heart, these electrical alternans are reflected in a beat-to-beat change of the T-wave segment of the electrocardiogram (ECG),[2] which is a global measure of the repolarization phase of the action potential of several billions of electrically coupled cells in the ventricles. Alternans have attracted widespread interest because of their close association with the onset of life-threatening ventricular arrhythmias and sudden cardiac death (SCD). Animal studies have shown that acute ischemia (i.e., a reduced blood supply) leads to large amplitude T-wave alternans that often precede the onset of ventricular fibrillation.[3] In addition, clinical studies have shown that human patients with even a very small level of T-wave alternans in the ECG are at higher risk for SCD.[4]

A well-known mechanism for producing temporal alternans is APD-restitution.[5,6] The end of an action potential is typically followed by a finite time interval until the next activation, which is necessary for the ventricles to fill with blood (diastolic filling) after a contraction. If this diastolic interval (DI) is short, cells lack sufficient time to fully recover their resting electrical properties before the next activation which then produces a shorter APD. Hence, the APD is typically an increasing function of DI at short DI and becomes constant at large DI. When the APD-restitution curve (APD vs DI) is steep, a small variation of DI produces a large variation of the next APD, and thus an even larger variation of the next DI at fixed pacing interval. Consequently, APD-restitution acts as an amplifier of small fluctuations of DI that produces an instability. The period doubling temporal nature of this instability was first demonstrated geometrically and mathematically in pioneering studies by Nolasco and Dahlen[5] and Guevara *et al.*,[6] respectively.

During one-dimensional circulation of an action potential in a ring of tissue, this same instability can lead to quasiperiodic oscillations of APD[7] that have been linked to conduction restitution (slowing of conduction at short DI).[8] The most relevant consequence of this instability for fibrillation, however, is in two (or more) spatial dimensions, where large

amplitude APD oscillations have been shown to cause spiral wave breakup and wave turbulence in numerical simulations.[9,10] Namely, if the APD is too large during an oscillation, the next DI can fall below some minimum value necessary for propagation of the next wave. Propagation failure then causes a local wave break that initiates new spirals, which may then break again by a similar mechanism.

This causal link between alternans and SCD is supported by recent experiments, which have found that flattening APD-restitution by drug intervention, which tends to suppress alternans in isolated cells, also tends to suppress fibrillation[11] and wavebreaks.[12] Further investigation of this link, however, remains presently necessary because APD oscillations in a regime of spiral wave turbulence are quite irregular and do not resemble simple temporal alternans. Hence, complex APD oscillations could also originate from different fibrillatory mechanisms that have been proposed.[13,14]

More recent experimental[15] and numerical[16] studies have demonstrated that pacing cardiac tissue can also initiate spirals via some intermediate state of discordant alternans. In this state, alternans have opposite phase in two juxtaposed regions of tissue, i.e., with a sequence of long-short-long-short APD in one region and short-long-short-long in the other. Therefore, on any given beat, a steep spatial gradient of APD is present along any path that crosses the boundary between these two regions. Such a gradient, in turn, facilitates retrograde propagation in a region of larger DI subsequent to propagation failure at a point of smallest DI, and hence the induction of reentry. Different mechanisms have been proposed to explain the formation of discordant alternans based on intrinsic spatial heterogeneity of repolarization[15,17] or conduction restitution.[16,18–20]

Over the last few years, several studies have demonstrated that temporal alternans can be suppressed by dynamic feedback control of the pacing interval.[21–25] This has been demonstrated for alternans in conduction time across the atrioventricular node, both *in vitro*[23] and in humans,[24] as well as *in vitro*[25] for APD-alternans. One interesting possibility is to use dynamic control to suppress APD-alternans in the human ventricles, and hence to potentially prevent SCD. This requires in principle to control alternans both temporally *and* spatially. Given the limited number of electrodes that can be realistically implanted in the ventricles, each pacing electrode should be able to suppress alternans in a finite volume of tissue. The central question becomes then, *what is the maximum volume of tissue within which alternans can be suppressed by a single electrode, and over what range of period*? The main goal of this paper is to provide a quantitative answer to this question in the simplest situation where the tissue is spatially homogeneous and alternans are a direct product of APD-restitution with negligible memory effects.

In the next section, we present the results of numerical simulations of the continuous cable equation. The main finding is that control is only effective up to a maximum tissue size that decreases sharply away from the alternans bifurcation point. This finding is then explained analytically in Sec. III by a linear stability analysis of a recently derived amplitude equation that governs the spatiotemporal dynamics of alternans near the onset of period doubling.[20] The results of this analysis are compared quantitatively to those of the cable equation simulations. The extension of these results to higher (two and three) spatial dimensions, which is directly relevant for control in the human ventricles, is then briefly discussed in Sec. IV, followed by conclusions in Sec. V.

II. NUMERICAL SIMULATIONS

We study the standard continuous cable equation defined by

$$\partial_t V = D\,\partial_x^2 V - (I_{\text{ion}} + I_{\text{ext}})/C_m\,, \tag{1}$$

where V is the transmembrane potential, I_{ion} is the total membrane ionic currents, C_m is the membrane capacitance, and $D \equiv 1/(\rho S C_m)$ is the diffusion constant of cardiac tissue that depends on the intracellular resistivity, ρ, and the cell surface to volume ratio, S. We consider a cable of length L and choose the external current I_{ext} to mimic a sequence of stimuli applied at one end of the cable, $x=0$. The interval T^n between the nth and nth$+1$ stimulus is determined by the dynamic control scheme

$$T^n = \tau + \frac{\gamma}{2}(\text{APD}^n - \text{APD}^{n-1}), \tag{2}$$

which is similar to the schemes used in previous studies of alternans control.[21–25] Here τ is the imposed pacing period and γ is a feedback gain parameter. For positive γ the second term on the right-hand side of Eq. (2) has the effect of lengthening the activation interval if the APD at the nth beat is larger than at the previous nth-1 beat. As a result, the following DI, and hence the next APD at the nth$+1$ beat, is larger than it would have been without control, which tends to suppress alternans.

We have simulated this control scheme for different ionic models and obtained qualitatively similar results. Therefore, for brevity, we only present results for the Noble model of the Purkinje fiber with I_{ion} defined in Ref. 26. The cable equation is discretized with a finite difference approximation of the spatial derivative with a mesh spacing $\Delta x = 0.01$ cm, and the resulting set of coupled differential equations is time stepped with a standard Euler scheme with a step $\Delta t = 0.05$ ms. We decrease τ in steps of 5 ms starting from a value where alternans are absent and give 200 stimuli for each value of τ. This procedure is repeated for different L up to 5 cm in increments of 0.5 cm. The APD is calculated at each point along the cable ($0 \leqslant x \leqslant L$) using $V = -40$ mV as threshold. When this procedure is carried out with control, the period is decreased from the largest τ with the control feedback always on.

We use for parameters $D = 2.5 \times 10^{-4}$ cm^2/ms and $C_m = 12\ \mu$F/cm^2. The value of the feedback gain is chosen to completely suppress temporal alternans for all pacing period in the zero-dimensional small L limit where the APD oscillations have the same amplitude and phase in the whole cable. In this limit, the dynamics is governed by Eq. (2) and $\text{APD}^{n+1} = f(T^n - \text{APD}^n)$, where $\text{APD} = f(\text{DI})$ is the APD-restitution curve that is plotted in Fig. 1(a). Using a linear

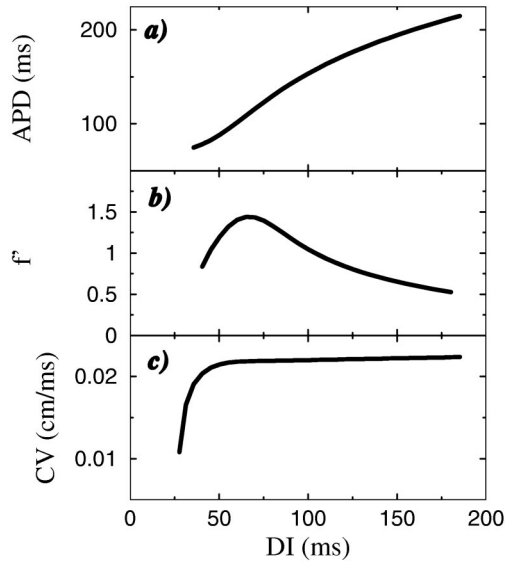

FIG. 1. Restitution curves of the Noble model computed by pacing a short cable with two stimuli and varying the time interval S1–S2 between them to vary DI. (a) APD-restitution curve, and its slope (b). (c) CV-restitution curve. $V=-40$ mV is used as threshold of the transmembrane potential to define the APD and DI.

stability analysis of this system of two coupled discrete maps,[23] it is straightforward to show that alternans are stabilized for

$$1-1/f'<\gamma<2/f', \tag{3}$$

where f' is the slope of f evaluated at the fixed point of the map. This condition implies that alternans can be suppressed up to a maximum slope $f'=3$ for the value of the gain parameter $\gamma=2/3$, as shown in Fig. 2. For the Noble kinetics, the maximum slope is only about 1.5 [Fig. 1(b)]. Therefore, we use in the simulations the value $\gamma=1/2$ that is sufficient to suppress temporal alternans for all pacing periods.

The results without and with control are summarized in Figs. 3(a) and 3(b), respectively. The main feature to note is

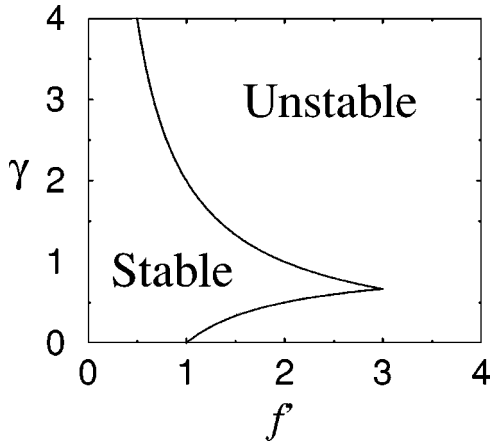

FIG. 2. Plot showing the stable region of the (γ,f') plane where control suppresses temporal alternans. γ is the strength of the feedback gain and f' is the slope of the APD-restitution curve. Zero-dimensional temporal alternans are suppressed for all pacing periods for the value $\gamma=1/2$ used in the Noble model simulations where the maximum slope is about 1.5.

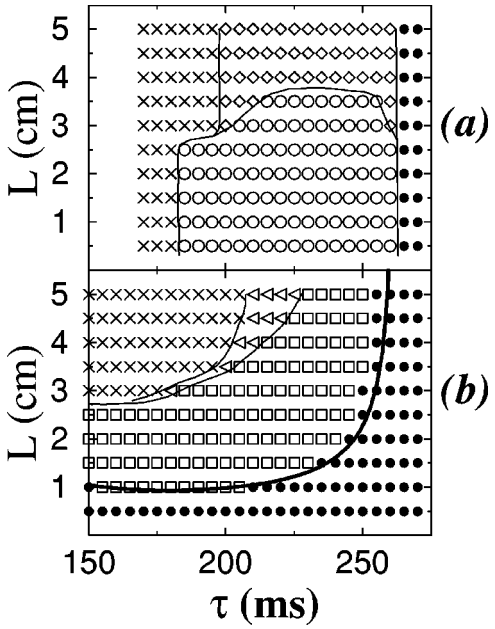

FIG. 3. Stability diagrams showing the regions of existence of different patterns of alternans in the plane of pacing period τ and cable length L for (a) $\gamma=0$ (without control) and (b) $\gamma=1/2$ (with control). The symbols in (a) and (b) correspond to no alternans (solid circles), concordant alternans with a nearly constant amplitude (open circles), first harmonic standing waves (open squares) that are only present when control suppresses the open circle concordant alternans, discordant stationary alternans (diamonds), traveling discordant alternans (triangles), and conduction block (crosses). The thin solid lines are guides to the eye. The thick solid line in (b) is the theoretical prediction for the onset of alternans with control [Eq. (16)].

that control is only effective up to some maximum cable length $L_{\max}$ that corresponds to the boundary between filled circles (no alternans) and open squares in Fig. 3(b). $L_{\max}$ is relatively small and constant over most of the range of τ, but increases rapidly as τ approaches the threshold period, $\tau_{\text{th}}(\gamma)$, for the onset of alternans in the large L limit. This critical period is between 250 and 255 ms for $\gamma=0.5$ in Fig. 3(b). Without control, this threshold period, $\tau_{\text{th}}(0)$, is between 260 and 265 ms in Fig. 3(a). Therefore, on the positive side, control is able to shift the onset of alternans in a long cable to a slightly shorter period. On the negative side, the maximum cable length for which control is effective (alternans are suppressed) drops rapidly as the period is decreased beyond this point.

The second main aspect of our results concerns the effect of control on the nature of the states of alternans. These states are illustrated in Figs. 4(a)–4(f) that show plots of APD profiles at two subsequent beats for different cable lengths and periods. Without control, concordant and discordant alternans are observed for small and large L, respectively. In the state of concordant alternans [Fig. 4(a)], the APD oscillates in phase (i.e., with the same sequence of long-short-long-short APD) in the whole cable and the APD is almost constant in space. In contrast, in the state of discordant alternans [Figs. 4(b)–4(c)], the two opposite ends of the cable oscillate with opposite phases and the APD vary rapidly in space across a node of constant APD, as found in recent studies without control.[16,18–20]

With control, a new state appears that is concordant, but

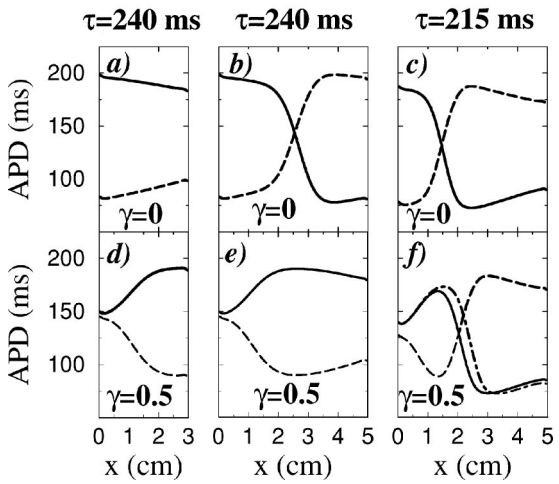

FIG. 4. Spatial profiles of APD during alternans. Profiles (a), (b), and (c) are without control ($\gamma=0$), and profiles (d), (e), and (f) are with control ($\gamma=0.5$) applied at $x=0$. In (a) through (e), the pattern of alternans are stationary and, accordingly, the solid and dashed lines show the APD at two subsequent beats. In (f), the pattern is traveling. This is illustrated by showing as a dash-dotted line the APD profile 50 beats ahead of the APD corresponding to the solid line; in (a) through (e) the dash-dotted and solid lines would coincide exactly.

which differs fundamentally from the state of concordant alternans without control in that the APD presents a more pronounced variation in space [Figs. 4(d) and 4(e)]. As explained in the next section, this state is directly analogous to the fundamental mode of standing sound waves in an open pipe and is termed here the ''first harmonic'' following this analogy. It is important to emphasize that this state only exists with dynamic control. Therefore, it should not be confused with the state of discordant alternans, even though the small amplitude near the pacing end of the cable appears to be similar to a node.

Finally, for large L outside the range shown in Fig. 3(b), the bifurcation to alternans with control is to a traveling state of discordant alternans. In the traveling state, node(s) form cyclically at the end of the cable distal from the paced end, and travel slowly across the cable toward the pacing site, where they disappear. This state is also present in the upper range of L shown here for small enough period [Fig. 4(f)]. We show in the next section that the transition from stationary to traveling discordant alternans, which is induced by control, is directly linked to the aforementioned shift of the bifurcation period of alternans [$\tau_{\rm th}(\gamma)<\tau_{\rm th}(0)$] for large L.

III. STABILITY ANALYSIS

A. Amplitude equation

We have recently derived an equation that describes the spatiotemporal dynamics of small amplitude alternans in paced cardiac tissue.[20] This amplitude equation can be quantitatively related to the cable equation (1) and its generalization to higher spatial dimensions close to the period doubling bifurcation point. That is, the choice of a particular form of $I_{\rm ion}$ in the cable equation only affects the values of coefficients that enter into the amplitude equation, but not the form of this equation. Furthermore, the latter can be treated analytically, which allowed us previously to obtain a simple understanding of the genesis of discordant alternans in the absence of control.[20]

Here, we extend this amplitude equation approach to include dynamic control in order to explain the results of the last section. This approach is based on writing the APD and the activation interval in the form

$$\mathrm{APD}^n \approx \mathrm{APD}_c + (-1)^n a, \tag{4}$$

$$T^n \approx \tau + (-1)^n b, \tag{5}$$

where APD_c is the APD at the period doubling bifurcation defined below by $\tau=\tau_c$, and a and b are amplitudes that vary slowly from beat to beat, with the fast oscillating part characteristic of alternans being factored out in the factor $(-1)^n$. Furthermore, in general both a and b can vary with position x along the cable. We showed previously that, in the absence of control, a and b obey the coupled set of equations

$$\tau\frac{\partial a}{\partial t}=\sigma a - b - w\frac{\partial a}{\partial x}+\xi^2\frac{\partial^2 a}{\partial x^2}, \tag{6}$$

$$b(x)=b(0)+\frac{1}{\Lambda}\int_0^x dx'\, a(x'), \tag{7}$$

where the time variable t, defined by $t\equiv n\tau$, can be treated as a continuous variable since the beat-to-beat variation of both a and b is slow, and we omit here nonlinear terms in a on the right-hand side (r.h.s.) of Eq. (6) since we are primarily interested in how the stability of the APD is influenced by control.

Let us briefly review the physical meaning of the various terms in the above equations and how they are obtained. The combination $\sigma a-b$ on the r.h.s. of Eq. (6) is a consequence of APD-restitution. Substituting Eqs. (4)–(5) in the second iteration of the map $\mathrm{APD}^{n+1}=f(T^n-\mathrm{APD}^n)$, one obtains $\partial a/\partial t=\sigma a-b$ with

$$\sigma=\ln(f')\approx f_c''(\tau-\tau_c)/2, \tag{8}$$

where $f'\equiv f'[\mathrm{DI}^*(\tau)]$ denotes the first derivative of f evaluated at the fixed point of the map, defined by $\mathrm{DI}^*(\tau)=\tau-\mathrm{APD}^*(\tau)$ and $\mathrm{APD}^*(\tau)=f[\tau-\mathrm{APD}^*(\tau)]$, and $f_c''\equiv f''[\mathrm{DI}^*(\tau_c)]$ is the second derivative of f evaluated at the period τ_c for which the slope of the restitution curve is unity; note that f_c'' is negative in the general case when the instability occurs by decreasing the period. This is the standard stability condition[5,6] for the alternans bifurcation in a small tissue patch where a is spatially uniform and $b=0$, in the absence of control. In such a tissue patch, APD oscillations become exponentially amplified, $a\sim\exp(\sigma t)$, when $\tau<\tau_c$, in which case $f'>1$ and $\sigma>0$. Note that τ_c is indistinguishable on the scale of Fig. 3(a) from the threshold period for alternans without control, $\tau_{\rm th}(0)$. We have shown previously that these two periods differ by an amount proportional to the slope of the conduction velocity (CV) restitution curve.[20] Since this slope is small for the Noble model [Fig. 1(c)], the difference between τ_c and $\tau_{\rm th}(0)$ is itself negligibly small.

The two spatial derivatives on the r.h.s. of Eq. (6) originate from the resistive electrical coupling between cells during repolarization, which tends to smooth out spatial varia-

tions of APD. Both first and second derivative terms are present because action potentials propagate in the $+x$ direction from the paced end of the cable toward the opposite end, and this propagation breaks the inherent parity symmetry $x \rightarrow -x$ that would be present if, for example, all the cells in the cable were activated simultaneously. It follows that the coefficient of the first derivative term, which explicitly breaks this symmetry, must vanish when the conduction velocity is infinite, and all the cells are effectively activated simultaneously, which implies the scaling $w \sim D/\mathrm{CV}$. Furthermore, since the second derivative term originates from the parity symmetric diffusive coupling in the cable equation, it follows that $\xi \sim (D \times \mathrm{APD}_c)^{1/2}$, which is essentially the length over which the membrane potential can diffuse on the characteristic time scale of repolarization. For typical parameters of cardiac tissue, ξ is a few mm and w is even smaller. The specific values obtained previously for the Noble model are $\xi = 0.18$ cm and $w = 0.045$ cm.[20]

Equation (7) is a direct consequence of the CV-restitution relationship: $\mathrm{CV} = c(\mathrm{DI})$. When the CV is constant, the interval between consecutive stimulations is the same for all cells along the cable, even when alternans are present. In contrast, when alternans are combined with CV-restitution, the CV will be larger on beats where the DI is large, following a short APD, than on the beats where the DI is small. This beat to beat oscillation of CV will in turn induce an oscillation of activation interval along the cable that is described by Eq. (7). The integral reflects the fact that the travel time of the action potential from the paced end to a given position x depends on the entire CV variation in between these two points. In addition, $\Lambda \equiv c^2/(2\,c')$ where c and its first derivative c' are evaluated at the fixed point of the map $\mathrm{DI}^*(\tau)$ defined above. This length is typically much larger than both ξ and w. This is especially true for the Noble model ($\Lambda = 49.1$ cm) because c' is small.

Without control, the activation interval at the paced end of the cable is equal to the drive period τ, which imposes the boundary condition $b(0,t) = 0$. With control, the activation interval at the paced end is defined by Eq. (2) and varies from beat to beat. Substituting Eqs. (4)–(5) into Eq. (2), it is simple to obtain the modified boundary condition

$$b(0,t) = \gamma a(0,t). \tag{9}$$

It is important to emphasize that control only enters the amplitude equation through this boundary condition. Finally, Eqs. (6), (7), and (9) can be combined into a single partial integro-differential equation for a

$$\tau \frac{\partial a}{\partial t} = \sigma a - w \frac{\partial a}{\partial x} + \xi^2 \frac{\partial^2 a}{\partial x^2} - \gamma a(0) - \frac{1}{\Lambda} \int_0^x dx'\, a(x'), \tag{10}$$

which is subject to the boundary condition $\partial a/\partial x = 0$ at the two ends of the cable.

B. Linear stability analysis

The effectiveness of control as a function of period and cable length, as well as its influence on the spatial patterns of alternans, can now be readily understood by a linear stability analysis of the amplitude equation (10). For this purpose, we substitute

$$a(x,t) = \exp(\Omega\, t/\tau)\, \Psi(x;\Omega), \tag{11}$$

in this equation, and look for solutions of the resulting eigenvalue problem that can be written in the form of a forced Helmholtz equation

$$\xi^2 \frac{d^2\Psi}{dx^2} + (\sigma - \Omega)\Psi = \gamma\Psi(0) + w \frac{d\Psi}{dx} + \frac{1}{\Lambda} \int_0^x dx'\, \Psi(x'), \tag{12}$$

subject to the boundary conditions

$$d\Psi/dx = 0, \ \text{at} \ x = 0, L. \tag{13}$$

A major simplification makes it possible to obtain a simple analytical solution to this eigenvalue problem for small L. Since the APD varies on a scale L with control, as seen in Figs. 4(d)–4(e), and, furthermore, $\xi \gg w$ and $\Lambda \gg \xi$, we can neglect the last two terms on the r.h.s. of Eq. (12) in the small L limit. Neglecting these two terms, the forcing becomes a constant, $\gamma\Psi(0)$, and the eigenvalues and eigenvectors are easily found to be

$$\Omega_0 = \sigma - \gamma, \ \text{with} \ \Psi_0 = A_0, \tag{14}$$

and

$$\Omega_n = \sigma - \frac{n^2\pi^2\xi^2}{L^2}, \ \text{with} \ \Psi_n = A_n \left[1 + \left(\frac{n^2\pi^2\xi^2}{\gamma L^2} - 1 \right) \cos\frac{n\pi x}{L} \right], \tag{15}$$

where $n \geq 1$ is an integer and A_0 and A_n are constants. More lengthy analytical expressions for Ω_n and Ψ_n obtained by retaining $w\, d\Psi/dx$ on the r.h.s. of Eq. (12), which are more accurate for intermediate L, are given in the Appendix.

Equation (14) is telling us something that we already know. Control stabilizes the state of concordant alternans with a spatially uniform APD. The bifurcation occurs when $\Omega_0 = 0$, or $\sigma = \gamma$ and $f' = \exp(\gamma)$ using Eq. (8). For the value $\gamma = 0.5$ used in the simulations, $f' = 1.648$. Since the maximum slope of the APD-restitution curve in the Noble model does not exceed this value [Fig. 1(b)], concordant alternans are always stable. In contrast, Eq. (15) is telling us something new. Namely, control fails to stabilize the harmonic modes of alternans, Ψ_n, since Ω_n is independent of the strength of the feedback gain γ! These modes become unstable when L is increased. The first mode to bifurcate is the largest wavelength first harmonic, Ψ_1. The bifurcation occurs when $\Omega_1 = 0$, or $L = L_{\max} = \pi\xi/\sqrt{\sigma}$, which defines the maximum cable length where alternans are suppressed by control. Using the definition of σ [Eq. (8)], we obtain the main result of this paper

$$L_{\max} \approx \xi \frac{2^{1/2}\,\pi}{[f_c''(\tau - \tau_c)]^{1/2}} \approx \xi \frac{\pi}{[\ln(f')]^{1/2}}, \tag{16}$$

where the second equality is valid over a wider range of τ because it does not involve expanding the slope $f'[\mathrm{DI}^*(\tau)]$ about τ_c. We plot $L_{\max}$ versus τ predicted by the second

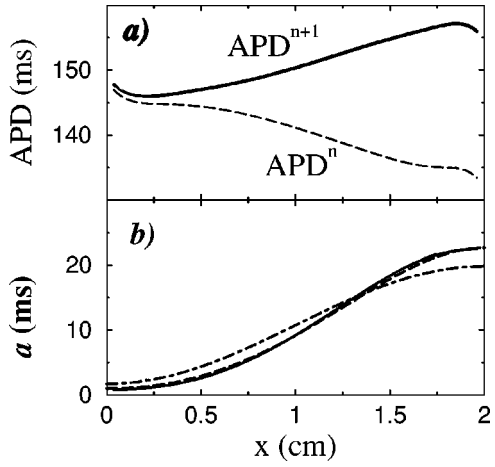

FIG. 5. Example of first harmonic standing wave for $\gamma=1/2$, $L=2$ cm, and $\tau=240$ ms. (a) shows the stationary APD profiles at two consecutive beats, APD^n (dashed line) and APD^{n+1} (solid line), in the cable equation simulation. (b) shows the comparison of their difference, $a\equiv \mathrm{APD}^{n+1}-\mathrm{APD}^n$ (solid line), with the theoretical predictions of the first harmonic amplitude given by Eq. (15) (dash-dotted line) and Eq. (A2) (dashed line). Note that the individual profiles of APD^n and APD^{n+1} become distorted by electrotonic effects at the two ends of the cable, which are asymmetrical at those ends in contrast to the interior of the cable. These distortions, however, vanish when the difference of these two profiles is evaluated to compute a that does indeed satisfy the zero slope boundary condition imposed on the amplitude equation.

equality in Eq. (16) as a thick solid line in Fig. 3(b). This line is seen to coincide well with the boundary between no alternans (solid circles) and the first harmonic mode (open squares), as expected. The first harmonic predicted by Eq. (15) [or the more accurate Eq. (A2) in the Appendix] with A_1 as a fit parameter are also found to agree well with the first harmonic observed in the cable equation simulation, as illustrated in Fig. 5. Note that this fit could be avoided by calculating A_1 from a weakly nonlinear analysis.

Equation (16) predicts that $L_{\max}$ diverges when τ approaches the threshold period of alternans without control, $\tau_c\approx\tau_{\mathrm{th}}(0)$, whereas in the simulations [Fig. 3(b)] $L_{\max}$ diverges at a threshold period with control, $\tau_{\mathrm{th}}(\gamma)$, which is shorter by a few ms for $\gamma=0.5$. This discrepancy is to be expected since Eq. (16) is only strictly valid for small L. The shift of $\tau_{\mathrm{th}}(\gamma)$ from τ_c can be explained by a numerical solution of Eq. (12) that includes all the forcing terms. This solution reveals that control destroys the state of stationary discordant alternans for large L when γ exceeds a small threshold. As a result, $\tau_{\mathrm{th}}(\gamma)$ is independent of γ above this threshold and is equal to the onset period for traveling discordant alternans without control that we have previously calculated,[20] or

$$\tau_c-\tau_{\mathrm{th}}(\gamma)\approx-\frac{3}{f_c''}\left(\frac{\xi}{2\Lambda}\right)^{2/3}. \tag{17}$$

This result has a simple physical interpretation which consists of two parts. First, control tends to suppress alternans at the pacing end ($x=0$), thereby trying to enforce a node at this point. In contrast, the state of stationary discordant alternans has an antinode at this same point. Therefore, control tends to suppress this state, and to replace it by a state of traveling discordant alternans that is compatible with a small amplitude of alternans at the paced end. Second, traveling states have an intrinsic wavelength $\lambda\sim(\xi^2\Lambda)^{1/3}$ that is shorter than the wavelength $\lambda\sim(w\Lambda)^{1/2}$ of the stationary states.[20] Since electrotonic effects are more effective at smoothing out spatial variations of APD on short length scales, the shorter wavelength traveling states require a steeper slope of the APD-restitution curve (and hence shorter period) to become destabilized. Note, however, that the difference between τ_c and $\tau_{\mathrm{th}}(\gamma)$ is typically small. It is predicted by Eq. (17) to be about 4 ms in the Noble model in agreement with the numerical results in the large L limit.

Finally, it is worth noting that stationary states of discordant alternans can be absent, already without control, when the slope of the CV-restitution curve near the onset of alternans is large enough.[20] In this case, the bifurcation period of alternans for large L is given by Eq. (17) both with and without control.

IV. DISCUSSION

Previous studies have shown that dynamic feedback control of the pacing interval can suppress temporal alternans over a wide range of pacing period for sufficient strength of feedback gain.[21–25] In this paper, we have investigated whether such a scheme can control alternans both temporally and spatially in a cable paced at one end.

Our main finding is that control is only effective up to maximum cable length, $L_{\max}$, where $L_{\max}$ increases rapidly as the pacing period approaches some threshold period that is independent of the value of the feedback gain (if not too small). This threshold period is close to, but shorter than the standard alternans bifurcation period corresponding to slope unity of the APD-restitution curve[5,6] by an amount proportional to the slope of the CV-restitution curve at the onset of alternans.[20]

We have shown that this maximum control length is directly linked to the existence of standing waves of alternans that are directly analogous to sound wave harmonics. Without control, the state of concordant alternans with a spatially uniform APD is the most unstable mode, and the higher order harmonics are more stable. Control, however, stabilizes concordant alternans, thereby making the first harmonic the first mode to bifurcate when the cable length exceeds some threshold that depends on the pacing period. In this mode, the amplitude of APD oscillation increases with distance away from the paced end.

Interestingly, the amplitude of alternans is small, albeit finite, at the paced end of the cable ($x=0$) where control is applied. It is important to emphasize that this failure of control to completely suppress alternans at this end is not a consequence of the finite accuracy of our numerical simulations. With our numerical scheme, control reduces the amplitude of alternans to a negligibly small value of the order of Δt in the zero-dimensional limit $L\to 0$. This value is typically one or two orders of magnitude smaller than the amplitude of alternans at the paced end obtained in the simulation of the finite L cable. The finiteness of this amplitude is analytically predicted by Eq. (15). Physically, it is simply a con-

sequence of the fact that all cells in the cable are electrically coupled. Hence, uncontrolled cells away from the paced end, which have a larger amplitude of APD oscillation, feed current to neighboring cells, thereby inducing a finite amplitude of oscillation at the paced end.

The finite accuracy in the measurement of the correct value of the feedback gain constitutes a source of noise in the system (unavoidable in experiments). Previous studies of spatiotemporal control in model systems of coupled chaotic maps have emphasized the importance of noise.[27–29] Here, we would expect the exponential amplification of noise to slightly increase the onset period of alternans in a large tissue [i.e., $\tau_{\mathrm{th}}(\gamma)\rightarrow\tau_c$] due to the convective nature of the instability that leads to traveling discordant alternans.[20] Furthermore, we would expect noise to smooth the bifurcation of the first harmonic mode without changing significantly the maximum control length.

Even though, for simplicity, we have focused on a one-dimensional cable geometry, the present results are straightforward to extend to higher spatial dimensions. For a two- or three-dimensional tissue paced from one site, stability is again governed by a forced Helmholtz equation similar to Eq. (12) with the second spatial derivative replaced by a d-dimensional Laplacian ($d=2,3$), a constant forcing term $\gamma\Psi(0)$ for small L, and a zero normal flux Neuman condition ($\partial\Psi/\partial n=0$) on the $d-1$ dimensional boundary of the tissue. Of course, the eigenvalues and eigenvectors will generally depend on the dimension and the shape of the tissue. However, the existence of a maximum control length and its rapid increase at a critical period should be universal features independent of dimension.

The existence of this length puts severe limitations on practical implementations of dynamic control. With one electrode controlling only $\sim 1\ \mathrm{cm}^3$ of tissue, the number of electrodes necessary to suppress alternans in the whole ventricles is probably unrealistically large. This number, however, may be reduced by only requiring control close to the onset of alternans, in which case the volume controlled by each electrode is larger. Clearly, the many technical difficulties involved in implementing dynamic control in the ventricles is far beyond the scope of the present paper whose main purpose has been to identify theoretical limitations of control from a single site.

In the present study, we have focused our attention on the simplest case where alternans are produced by APD-restitution, with the APD determined predominantly by the previous DI. In contrast, Hall and Gauthier have recently found that this assumption is insufficient to model quantitatively their experimental data on temporal alternans.[25] In particular, these authors found that the slope of the APD restitution curve at the onset of alternans is significantly larger than unity in their experiments, which conflicts with the slope unity prediction of the standard map $\mathrm{APD}=f(\mathrm{DI})$. They have used a two-dimensional map[30] with a phenomenological incorporation of memory effects that predicts well the structure of the alternans bifurcation in the absence of control, but not with control. The study of Hall and Gauthier, and others,[30,31] indicate that temporal alternans generally need to be modeled by more complex maps than the one considered here, which remain to be developed. However, the universality of the amplitude equation description leads us to expect that the main features of our results will remain valid for such maps, in particular the existence of standing wave modes that limit the spatial extent of control.

Finally, the present study suggests that dynamic control can provide a valuable experimental probe of alternans. In particular, from the amplitude equation study, ξ emerges as a crucial length scale controlling the spatiotemporal dynamics of both concordant and discordant alternans.[20] This length is difficult to extract experimentally. However, the bifurcation period and the shape of the first harmonic mode depend sensitively on ξ. Therefore, pacing cardiac tissue in a way that makes alternating rhythms resonate like sound waves should make it possible to extract this crucial length scale. In addition, it should help to enlarge our fundamental understanding of these rhythms.

V. CONCLUSIONS

We have studied the spatiotemporal control of alternans in paced cardiac tissue by both cable equation simulations and a linear stability analysis of a recently derived amplitude equation.[20] Our main finding is that control is only effective up to a maximum tissue size that drops sharply beyond the threshold period for alternans in a large tissue. We have shown that the existence of this maximum size is due to the failure of control to stabilize standing wave modes of alternans that are analogous to sound harmonics. We expect the existence of these modes to be a universal feature of spatiotemporal control of alternans from a single point that should be directly observable experimentally.

ACKNOWLEDGMENTS

This research was supported in part by NIH SCOR in Sudden Cardiac Death P50-HL52319 and benefited from allocation of computer time at the NU-ASCC.

APPENDIX

An exact analytical solution of Eq. (12) can be obtained in the limit $\Lambda\rightarrow+\infty$ of no CV-restitution. The corresponding eigenvalues and eigenvectors are

$$\Omega_n=\sigma-\frac{n^2\pi^2\xi^2}{L^2}-\frac{w^2}{4\xi^2}, \tag{A1}$$

and

$$\Psi_n=A_n\left\{e^{wx/2\xi^2}\left[\frac{1}{\gamma}\left(\frac{n^2\pi^2\xi^2}{L^2}+\frac{w^2}{4\xi^2}\right)-1\right]\times\left(\cos\frac{n\pi x}{L}-\frac{wL}{2n\xi^2\pi}\sin\frac{n\pi x}{L}\right)+1\right\}, \tag{A2}$$

respectively. When $wL/(2n\pi\xi^2)\ll 1$ the former expression reduces to Eq. (15).

[1] G. R. Mines, J. Physiol. (London) **46**, 349 (1913).
[2] T. Lewis, Q. J. Med. **4**, 141 (1910).
[3] B. Nearing, A. H. Huang, and R. L. Verrier, Science **252**, 437 (1991).
[4] D. S. Rosenbaum, L. E. Jakson, J. M. Smith, H. Garam, J. N. Ruskin, and R. J. Cohen, N. Engl. J. Med. **330**, 235 (1994).

[5] J. B. Nolasco and R. W. Dahlen, J. Appl. Physiol. **25**, 191 (1968).
[6] M. R. Guevara *et al.*, in *Computers in Cardiology* (IEEE Computer Society, New York, 1984), p. 167.
[7] L. H. Frame and M. B. Simson, Circulation **78**, 1277 (1988).
[8] M. Courtemanche, L. Glass, and J. P. Keener, Phys. Rev. Lett. **70**, 2182 (1993).
[9] A. Karma, Chaos **4**, 461 (1994).
[10] J. N. Weiss, A. Garfinkel, H. S. Karaguezian, Z. Qu, and P.-S. Chen, Circulation **99**, 2819 (1999).
[11] M. L. Riccio, M. L. Koller, and R. F. Gilmour, Jr., Circ. Res. **84**, 955 (1999).
[12] A. Garfinkel, Y.-H. Kim, O. Voroshilovsky, Z. Qu, J. R. Kil, M.-H. Lee, H. S. Karaguezian, J. N. Weiss, and P.-S. Chen, Proc. Natl. Acad. Sci. U.S.A. **97**, 6061 (2000).
[13] J. M. Rogers and R. E. Ideker, Circ. Res. **86**, 369 (2000).
[14] A. V. Zaitsev, O. Berenfeld, S. F. Mironov, J. Jalife, and A. M. Pertsov, Circ. Res. **86**, 408 (2000).
[15] J. M. Pastore, S. D. Girouard, K. R. Laurita, F. G. Akar, and D. S. Rosenbaum, Circulation **99**, 1385 (1999).
[16] Z. Qu, A. Garfinkel, P.-S. Chen, and J. W. Weiss, Circulation **102**, 1664 (2000).
[17] D. S. Rosenbaum, J. Cardiovasc. Electrophysiol. **12**, 207 (2001).
[18] M. A. Watanabe, F. H. Fenton, S. J. Evans, H. M. Hastings, and A. Karma, J. Cardiovasc. Electrophysiol. **12**, 196 (2001).
[19] J. J. Fox, M. L. Riccio, F. Hua, E. Bodenschatz, and R. F. Gilmour, Circ. Res. **90**, 289 (2002).
[20] B. Echebarria and A. Karma, Phys. Rev. Lett. **88**, 208101 (2002).
[21] D. J. Christini and J. J. Collins, Phys. Rev. E **53**, R49 (1996).
[22] D. J. Gauthier and J. E. S. Socolar, Phys. Rev. Lett. **79**, 4938 (1997).
[23] K. Hall, D. J. Christini, M. Tremblay, J. J. Collins, L. Glass, and J. Billette, Phys. Rev. Lett. **78**, 4518 (1997).
[24] D. J. Christini, K. M. Stein, S. M. Markowitz, S. Mittal, D. J. Slotwiner, M. A. Scheiner, S. Iwai, and B. B. Lerman, Proc. Natl. Acad. Sci. U.S.A. **98**, 5827 (2001).
[25] G. M. Hall and D. Gauthier, Phys. Rev. Lett. **88**, 198102 (2002).
[26] D. Noble, J. Physiol. **160**, 317 (1962).
[27] D. Auerbach, Phys. Rev. Lett. **72**, 1184 (1994).
[28] R. O. Grigoriev, M. C. Cross, and H. G. Schuster, Phys. Rev. Lett. **79**, 2795 (1997).
[29] D. A. Egolf and J. E. S. Socolar, Phys. Rev. E **57**, 5271 (1998).
[30] D. R. Chialvo, D. C. Michaels, and J. Jalife, Circ. Res. **66**, 525 (1990).
[31] R. F. Gilmour, Jr., N. F. Otani, and M. A. Watanabe, Am. J. Physiol. **272**, H1826 (1997).